Tractable Data Enriched Distributionally Robust Chance-Constrained Conservation Voltage Reduction

Qianzhi Zhang, *Member, IEEE,* Fankun Bu, *Graduate Student Member, IEEE,* Yi Guo, *Member, IEEE,* and Zhaoyu Wang, *Senior Member, IEEE,*

***Abstract*—This paper proposes a tractable distributionally robust chance-constrained conservation voltage reduction (DRCC-CVR) method with enriched data-based ambiguity set in unbalanced three-phase distribution systems. The increasing penetration of distributed renewable generation not only brings clean power but also challenges the voltage regulation and energy-saving performance of CVR by introducing high uncertainties to distribution systems. In most cases, the conventional robust optimization methods for CVR only provide conservative solutions. To better consider the impacts of load and PV generation uncertainties on CVR implementation in distribution systems and provide less conservative solutions, this paper develops a data-based DRCC-CVR model with tractable reformulation and data enrichment method. Even though the uncertainties of load and photovoltaic (PV) can be captured by data, the availability of smart meters (SMs) and micro-phasor measurement units (PMUs) is restricted by cost budget. The limited data access may hinder the performance of the proposed DRCC-CVR. Thus, we further present a data enrichment method to statistically recover the high-resolution load and PV generation data from low-resolution data with Gaussian Process Regression (GPR) and Markov Chain (MC) models, which can be used to construct a data-based moment ambiguity set of uncertainty distributions for the proposed DRCC-CVR. Finally, the nonlinear power flow and voltage dependant load models and DRCC with moment-based ambiguity set are reformulated to be computationally tractable and tested on a real distribution feeder in Midwest U. S. to validate the effectiveness and robustness of the proposed method.**

***Index Terms*—Conservation voltage reduction, data enhancement, distributionally robust chance-constrained optimization, distribution systems, tractable reformulation.**

I. Nomenclature

Sets and Indices

$\mathcal{N}, i, j$	Set and indices of buses.
$\mathcal{E}, ij$	Set of branches and index of branch between bus i and bus j..
$\mathcal{G}$	Set of PV generators.
$\mathcal{D}_\xi$	Ambiguity set of uncertainty.
s	Index of service transformer.
m	Index of data sample.
t	Index of time instant.
ϕ	Index of three-phase ϕ_a, ϕ_b, ϕ_c.

Parameters

A_0, A	Topology matrices of a radial distribution network.
D_r, D_x	Block diagonal matrices of line segment resistance and reactance.
k_1^p, k_2^p, k_3^p	Constant-impedance, -current and -power coefficients for active ZIP load.
k_1^q, k_2^q, k_3^q	Constant-impedance, -current and -power coefficients for reactive ZIP load.
N	Total bus number.
$\overline{P}(t), \underline{P}(t)$	Upper and lower bounds of instantaneous load/renewable generation within the t-th hour.
$P_a(t)$	Average load/renewable generation over the t-th hour.
$p^{\mathrm{g}}_{i,\phi,t}$	Three-phase deterministic active power injections by the PV inverter at bus i, phase ϕ and time t.
$t^{\mathrm{PL}}_{i,\phi,t}, t^{\mathrm{QL}}_{i,\phi,t}$	Deterministic active and reactive load shape multipliers at bus i, phase ϕ and time t.
$s^{\mathrm{cap}}_{i,\phi,t}$	Power capacity of PV inverters at bus i, phase ϕ and time t.
R, X	Sensitive Matrices with line resistance and reactance.
$\bar{r}_{ij}, \bar{x}_{ij}$	Matrices of the line resistance and reactance over line ij in the unbalanced three-phase distribution systems.
$v^{\min}, v^{\max}$	Minimum and maximum limits for squared nodal voltage magnitude.
v_0, v	Vector of squared nodal voltage magnitudes.
$\Delta V, \Delta v$	Vector of voltage and squared voltage deviations.
ϵ	Pre-defined risk level in chance constraints.
$\varepsilon^p_{ij,\phi,t}, \varepsilon^q_{ij,\phi,t}$	Active and reactive power loss nonlinear terms at line ij, phase ϕ and time t.
$\varepsilon^v_{i,\phi,t}$	Voltage drop nonlinear term at bus i, phase ϕ and time t.

Variables

$P_{ij,\phi,t}, Q_{ij,\phi,t}$	Three-phase active and reactive power flows at line ij, phase ϕ and time t.
P, Q	Vector of active and reactive line power flows.
p, q	Vector of active and reactive nodal power injec-

This work was supported in part by the U.S. Department of Energy Wind Energy Technologies Office under Grant DE-EE0008956, and in part by the National Science Foundation under ECCS 1929975. This work was partially supported by an ETH Zürich Postdoctoral Fellowship. (*Corresponding author: Zhaoyu Wang*).

Qianzhi Zhang, Fankun Bu, and Zhaoyu Wang are with the Department of Electrical and Computer Engineering, Iowa State University, Ames, IA 50011 USA (e-mail: qianzhi@iastate.edu; fbu@iastate.edu; wzy@iastate.edu).

Yi Guo is with Power Systems Laboratory at ETH Zürich, Zürich, 8092, Switzerland (e-mail: guo@eeh.ee.ethz.ch).

tions.

$p^{\mathrm{g}}, q^{\mathrm{g}}$	Vector of active and reactive PV generations.
$p^{\mathrm{ZIP}}, q^{\mathrm{ZIP}}$	Vector of active and reactive ZIP loads.
$t^{\mathrm{PL},\xi}_{i,\phi,t}, t^{\mathrm{QL},\xi}_{i,\phi,t}$	Three-phase active and reactive load shape multipliers at bus i, phase ϕ and time t.
$p^{\mathrm{g},\xi}_{i,\phi,t}$	Three-phase active power injections by the PV inverter at bus i, phase ϕ and time t.
$p^{\mathrm{ZIP}}_{i,\phi,t}, q^{\mathrm{ZIP}}_{i,\phi,t}$	Three-phase active and reactive ZIP loads at bus i, phase ϕ and time t.
$q^{\mathrm{g}}_{i,\phi,t}, Q^{\mathrm{cap}}_{i,\phi,t}$	Three-phase reactive power injections and power capacity of PV inverters at bus i, phase ϕ and time t.
$S_{ij,\phi,t}$	Three-phase apparent power flow at line ij, phase ϕ and time t.
$v_{i,\phi,t}$	Squared of three-phase voltage magnitude at bus i, phase ϕ and time t.
x	Vector of decision variables.
$\alpha^{\mathrm{q}}_{i,\phi,t}$	Ratio between PV reactive power output and PV reactive capacity at bus i, phase ϕ and time t.
ξ	Compact vector collecting of all uncertain parameters.
μ, Σ	Mean and covariance of the uncertain variables of load and PV generation.

Functions

GPR^*_s	GPR function for the s-th teacher service transformer.
MC^*_s	Second-order MC function for the s-th teacher service transformer.
Be	Bermouli distribution function.

II. Introduction

CONSERVATION voltage reduction (CVR) can reduce the voltage for peak load shaving and long-term energy-saving [1]. To achieve system-wide optimal performance, voltage/var optimization-based CVR (VVO-CVR) is previously studied [1]–[4], which can be cast into an optimal power flow program. While the previous works have contributed valuable insights to VVO-CVR, there are problems remaining open, summarized as follows:

(1) *The impact of load and renewable generation uncertainties on VVO-CVR:* In [2], a linear least-squares centralized optimization model is developed for coordinating combinations of voltage regulating devices and PVs to implement CVR in distribution systems. In [3] and [4], several alternating direction method of multipliers (ADMM)-based distributed optimization algorithms are developed for CVR implementation, which can decompose a large-scale VVO-CVR problem into several small-scale problems with improved scalability. However, the above centralized or distributed VVO-CVR works [2]–[4] are developed based on deterministic optimization methods, which assume the perfect forecasts of load and renewable generation. Neglecting those prediction errors could result in potential violations of operational constraints, such as bus voltage constraints in VVO-CVR. To consider the impacts of load and renewable generation uncertainties on voltage regulation for CVR implementation, stochastic programming (SP) and robust optimization (RO) are applied in some existing works [5]–[8]. In [5] and [6], the scenario-based SP methods aim at optimizing reactive power dispatch for voltage regulation with expected performance and an accurate probability distribution model. While the SP methods need an accurate probability distribution model and a large sampling number of scenarios, it requires heavy computational efforts. In [7] and [8], the RO methods are developed to handle the uncertain load and renewable generation production. However, the RO methods can only give a feasible solution for the worst-case scenario, which is too conservative and hinders the performance of CVR.

In recent years, the distributionally robust optimization (DRO) has been considered a more effective way to handle uncertainty in multiple power systems applications, such as economic dispatch [9]–[11], power dispatch [12]–[16], unit commitment [17]–[19], and voltage regulation and reactive power control [20], [21]. The DRO techniques construct an ambiguity set of probability distributions based on historical data, including all possible uncertainty distributions. Thus, the DRO can ensure that the operational constraints can be satisfied for any distributions in the ambiguity set built upon the moments of a probability distribution or structural information. In general, the ambiguity set of DRO can be constructed by the moment-based method and metric-based ambiguity set [15]. For example, the first two moments (e.g., mean and variance) are used to build moment-based ambiguity set in [9], [10], [12], [13], [20]. Another type of ambiguity set is constructed by the metric-based method [11], [16]–[19], [21], where the possible distributions are centered at the reference distribution with a certain distance metric based on the training samples. The key idea behind CVR implementation is load demand reduction. Therefore, we need to consider not only the uncertainty of renewable generation but also the uncertainty of load demand. However, some existing metric-based DRO works [11], [16]–[19], [21] only consider the uncertainty of renewable generation, while the uncertainty of load demand is neglected. If multiple uncertainties are considered, the metric-based method may need more data samples than the moment-based method to construct ambiguity sets. Conversely, the moment-based DRO methods can construct the ambiguity set of multiple uncertainties with a reasonable assumption of distribution [22]. Most of the DRO methods based on metric-based ambiguity set are computational intractability and need relaxation transformation to obtain trackable models [23], such as KL-diverge and Wasserstein metric ball, which may lead to an infeasible solution [20]. The computational burden of the metric-based DRO model grows heavily with the number of employed data [24]. Also, data privacy is another concern in the metric-based method because all the data need to be broadcasted to each agent in the system. On the other side, the moment-based DRO model can construct the ambiguity set with the moment information more straightforwardly. Furthermore, we incorporate the data enrichment method to strengthen the moment-based ambiguity set and reduce the conservativeness of DRO solutions. Therefore, to take both load and renewable generation uncertainties into account and consider the tradeoff between computational cost and data availability, we choose the moment-based method to construct an ambiguity set for CVR implementation.

Lately, the distributionally robust chance-constrained (DRCC) models [25], [26] are developed by integrating the chance constraints in DRO to enforce certain events within a probability threshold. Even though DRO and DRCC models have some advantages over conventional deterministic and stochastic approaches, there are still challenges to using the DRCC method for CVR implementation, including how to formulate DRCC in a tractable way for CVR implementation and how to construct an ambiguity set with limited access to historical and real-time load/PV data.

(2) *Availability of data for constructing ambiguity set of load and renewable generation uncertainties:* Even though the ambiguity set of uncertainty in DRCC can characterize a group of possibility distributions, defining a high-quality ambiguity set is non-trivial, as one needs to decide the tradeoff between the conservativeness of decisions and the operational efficiency, while considering the mathematical tractability. To construct an ambiguity set of uncertainties in DRCC, the conventional way is using statistical inference and data analysis methods with the historical data and system feedback measurements. For example, the existing DRO works [27] and [28] use data-based method to construct ambiguity set. However, the aforementioned data-based ambiguity set relies heavily on either sufficiently high-resolution data or complex machine learning methods.

(3) *Intractable DRCC and nonlinear voltage-dependent load models:* The VVO-CVR problem is nonlinear and intractable, which makes a distributionally robust stochastic reformulation of the VVO-CVR problem even more challenging. In [29], an approximation method is proposed for conventional DRO problems, while the approximation for DRCC problems is not considered. Also, the loads are considered as voltage-independent models in above reference of DRO and DRCC [12], [13], [25], [26]. In practice, the nature of CVR is lowering network voltages to reduce the voltage, and the literature on the CVR problem validates the necessity of voltage-dependent loads, such as ZIP load and exponential load models [3]. In existing research works [30] and [31], some approximation methods are applied to linearize ZIP load model in deterministic optimization. However, the linearization and convexification for ZIP load model in DRO or DRCC with uncertainties of load are not considered in previous works [12], [13], [25], [26], [29]–[31].

To capture the uncertainties of load and PV generation through data-based methods in modern distribution networks, micro-phasor measurement units (PMUs) and smart meters (SMs) are implemented to record load and PV generation data, where micro-PMUs[1] can record high-resolution data (1-second resolution or higher), and SMs[2] can record low-resolution data (typically 1-hour resolution). However, due to the cost issue, micro-PMUs are only installed at limited locations in real distribution networks, while SMs are widely installed in real distribution networks. Therefore, the access to available data for constructing an ambiguity set is limited by the number of micro-PMUs and SMs. If we only use limited data to construct an ambiguity set, it may hinder the performance of the DRCC program. The data from SMs and micro-PMUs are necessary but need modification to support our proposed method. Therefore, we need to enrich the load and PV generation data, then construct the data-based ambiguity set for uncertainties of load and PV generation.

To address the above challenges, this paper proposes a tractable data-based DRCC-CVR model under the uncertainties of voltage-dependent load and PV generation. Inspired by our previous work [32], we apply the data enrichment method to both load and PV generation data from SMs and micro-PMU, then construct the ambiguity set of uncertainties with the enriched data for the proposed DRCC-CVR. This data enrichment method enables a strong connection between the moment-based representation of the limited data set and the moment-based ambiguity set of the DRCC model, which avoids over- or under-conservativeness of the decisions. The main contributions of this paper are three-fold:

- *DRCC-CVR model with uncertainties of load and solar PV generation:* To consider the impacts of load and renewable uncertainties on voltage regulation and energy-saving performance of CVR in the unbalanced three-phase distribution systems, we present a deterministic VVO-CVR model and extend it by introducing chance constraints for possible voltage violations due to the load and the renewable uncertainties. To obtain proper conservative solutions robust to the high-resolution dataset and ensure a better performance for energy-saving and voltage regulation of CVR, we further integrate the chance constraints with DRO techniques to propose a DRCC-CVR model. We choose the moment-based method to construct an ambiguity set for CVR implementation to consider both load and renewable generation uncertainties and the tradeoff between the computational cost and the data availability.
- *Data enrichment method with limited SM and micro-PMU data:* To guarantee the performance of the data-based DRCC-CVR model, we leverage the data enrichment method to recover the high-resolution load and PV generation data from SMs and micro-PMUs. The moment information of load and PV generation uncertainties are extracted from the enriched data to construct the moment-based ambiguity sets for the proposed DRCC-CVR model. The proposed data enrichment can enhance the relationship between the statistical information of historical data and CVR implementation.
- *Tractable reformulation of the DRCC-CVR model:* To make our proposed DRCC-CVR model tractable, we first present the linearized version of the power flow model and voltage-dependent ZIP load model that can relieve the computational burden of the proposed DRCC-CVR model. Then, we build an ambiguity set with the first two moment information of load and PV generation probability distributions extracted from the enriched data and

[1]Micro-PMUs are synchrophasor devices that high-speed record real-time stamped data measurement of power and energy consumption. Micro-PMUs have a high sampling rate, e.g., one sample per second or higher [32]

[2]SMs are electronic devices that record power and energy consumption and can communicate remotely with utility. SMs have a relatively low sampling rate compared to micro-PMUs, e.g., one sample per hour [32].

input this moment-based ambiguity set of load and PV generation uncertainties for a tractable reformulation of DRCC-CVR.

The remainder of the paper is organized as follows: Section III discusses the challenges of a classical VVO-CVR and its DRCC-CVR reformulation and shows the overall framework of our proposed method. Section IV presents the linearized power flow model and voltage-dependent ZIP load model and shows the tractable reformulation of DRCC-CVR. Section V introduces a data enrichment method with high-resolution micro-PMU data and low-resolution SM data and constructs the data-based moment-based ambiguity set. Simulation results and conclusions are given in Section VI and Section VII, respectively.

III. The Problem Formulation and the Proposed Method

A. Solving a VVO-CVR Problem in the Unbalanced Three-phase Distribution Networks

In this paper, we consider an unbalanced three-phase radial distribution network that consists of N buses denoted by a set $\mathcal{N}$ and $N-1$ branches denoted by a set $\mathcal{E}$. Let $bp(i)$ denote the bus that immediately precedes bus i along the radial network headed by the feeder head bus. The three-phase indices ϕ_a, ϕ_b, ϕ_c are simplified as ϕ. The time instance is represented by t. Distributed assets are located at different buses, including voltage-dependent ZIP loads and solar PV distributed generators. We assume that the customers are either equipped with SMs or micro-PMUs, which monitor the active and reactive load power and active PV generation power with proper time resolution. For each bus $i \in \mathcal{N}$, let $p^{\text{ZIP}}_{i,\phi,t}, q^{\text{ZIP}}_{i,\phi,t} \in \mathbb{R}^{3\times 1}$ denote the vector of three-phase active and reactive voltage-dependent ZIP loads at time t. For each bus $i \in \mathcal{G}$, let $p^{\text{g}}_{i,\phi,t}, q^{\text{g}}_{i,\phi,t} \in \mathbb{R}^{3\times 1}$ denote the vector of three-phase active and reactive power outputs of the i-th PV inverter at time t; $V_{i,\phi,t} \in \mathbb{R}^{3\times 1}$ represents the vector of three-phase voltage magnitude at time t, $v_{i,\phi,t} := V_{i,\phi,t} \odot V_{i,\phi,t} \in \mathbb{R}^{3\times 1}$ represents the vector of three-phase squared voltage magnitude at time t. For each branch $(i,j) \in \mathcal{E}$, let $z_{ij} = r_{ij} + \mathbf{i}x_{ij} \in \mathbb{C}^{3\times 3}$ denotes matrix of the three-phase impedance of line ij, where r_{ij} and x_{ij} are the matrices of the three-phase resistance and reactance, respectively. Let $S_{ij,\phi,t} = P_{ij,\phi,t} + \mathbf{i}Q_{ij,\phi,t} \in \mathbb{C}^{3\times 1}$ denotes the vector of three-phase apparent power, where $P_{ij,\phi,t}$ and $Q_{ij,\phi,t}$ are the vector of three-phase active and reactive power flow through line ij from bus i to bus j at time t. Let the line active and reactive power flows, nodal active and reactive power injections, and squared voltage magnitudes be denoted by the following column vectors: $P = \{P_{bp(i)i,\phi,t}, \forall i,t,\phi\}$, $Q = \{Q_{bp(i)i,\phi,t}, \forall i,t,\phi\}$, $p = \{p_{i,\phi,t}, \forall i,t,\phi\}$, $q = \{q_{i,\phi,t}, \forall i,t,\phi\}$, and $v = \{v_{i,\phi,t}, \forall i,t,\phi\}$. $\odot$ and $\oslash$ denote the element-wise multiplication and division.

The classic VVO-CVR program can be formulated as a deterministic problem (1), which aims to reduce the total power consumption of the entire distribution network while maintaining a feasible voltage profile within the predefined bounds across the distribution network as follows:

$$\min_{P,Q,p,q,v} \sum_{t\in[t,t+T]} \sum_{j:0\to j} \sum_{\phi\in\{\text{a,b,c}\}} \text{Re}\{S_{0j,\phi,t}\}, \tag{1a}$$

s.t.

$$P_{ij,\phi,t} = \sum_{k:j\to k} P_{jk,\phi,t} - p^{\text{g}}_{j,\phi,t} + p^{\text{ZIP}}_{j,\phi,t} + \varepsilon^{p}_{ij,\phi,t}, \tag{1b}$$

$$Q_{ij,\phi,t} = \sum_{k:j\to k} Q_{jk,\phi,t} - q^{\text{g}}_{j,\phi,t} + q^{\text{ZIP}}_{j,\phi,t} + \varepsilon^{q}_{ij,\phi,t}, \tag{1c}$$

$$v_{j,\phi,t} = v_{i,\phi,t} - 2\big(\bar{r}_{ij} \odot P_{ij,\phi,t} + \bar{x}_{ij} \odot Q_{ij,\phi,t}\big) + \varepsilon^{v}_{i,\phi,t}, \tag{1d}$$

$$p^{\text{ZIP}}_{i,\phi,t} = t^{\text{PL}}_{i,\phi,t} \odot \big(k^{p}_{i,1} \cdot v_{i,\phi,t} + k^{p}_{i,2} \cdot \sqrt{v_{i,\phi,t}} + k^{p}_{i,3}\big), \tag{1e}$$

$$q^{\text{ZIP}}_{i,\phi,t} = t^{\text{QL}}_{i,\phi,t} \odot \big(k^{q}_{i,1} \cdot v_{i,\phi,t} + k^{q}_{i,2} \cdot \sqrt{v_{i,\phi,t}} + k^{q}_{i,3}\big), \tag{1f}$$

$$-Q^{\text{cap}}_{i,\phi,t} \le qg_{i,\phi,t} \le Q^{\text{cap}}_{i,\phi,t}, \forall i \in \mathcal{G}, \tag{1g}$$

$$Q^{\text{cap}}_{i,\phi,t} = \sqrt{(S^{\text{cap}}_{i,\phi,t})^2 - (p^{\text{g}}_{i,\phi,t})^2}, \forall i \in \mathcal{G}, \tag{1h}$$

$$v^{\min} \le v_{i,\phi,t} \le v^{\max}, \forall i \in \mathcal{N}. \tag{1i}$$

In objective function (1a), the three-phase active power supplied from the substation of the feeders $\text{Re}\{S_{0j,\phi,t}\}$ is minimized over a moving finite horizon $[t, t+T]$ for energy-saving with CVR implementation. Constraints (1b)-(1d) are defined by the unbalanced three-phase version of DistFlow model [3]. Constraints (1b) and (1c) guarantee the nodal active and reactive power balance. Constraint (1d) calculates the voltage difference between bus i and bus j. The detailed formulations of nonlinear terms $\varepsilon^{p}_{ij,\phi,t}$, $\varepsilon^{q}_{ij,\phi,t}$ and $\varepsilon^{v}_{i,\phi,t}$ can be found in [4]. If the network is not too severely unbalanced, the voltage magnitudes between the phases are similar, and the relative phase unbalance is small [3], then we can use the unbalanced three-phase resistance matrix $\bar{r}_{ij}$ and reactance matrix $\bar{x}_{ij}$ in constraint (1d). More details about $\bar{r}_{ij}$ and $\bar{x}_{ij}$ for unbalanced three-phase distribution systems can be referred to [3]. The implementation of CVR requires the modeling of voltage-dependent ZIP active and reactive loads $p^{\text{ZIP}}_{i,\phi,t}$ and $q^{\text{ZIP}}_{i,\phi,t}$, as shown in (1e) and (1f). $t^{\text{PL}}_{i,\phi,t}, t^{\text{QL}}_{i,\phi,t} \in \mathbb{R}^{3\times 1}$ are the vectors of three-phase active and reactive load shape multipliers on bus i at time t, respectively. Note that $t^{\text{PL}}_{i,\phi,t} \in [0,1]$ and $t^{\text{QL}}_{i,\phi,t} \in [0,1]$ are two regularized vectors, which represent the shapes of active and reactive load demands. $k^{p}_{i,1}$, $k^{p}_{i,2}$, $k^{p}_{i,3}$ and $k^{q}_{i,1}$, $k^{q}_{i,2}$, $k^{q}_{i,3}$ are constant-impedance (Z), constant-current (I) and constant-power (P) coefficients for active and reactive ZIP loads on bus i. Constraint (1g) limits the reactive power output $q^{\text{g}}_{i,\phi,t}$ of the PV inverters by the available reactive power capacity $Q^{\text{cap}}_{i,\phi,t}$. Constraint (1h) calculates $Q^{\text{cap}}_{i,\phi,t}$ with the total capacity of the PV inverter $S^{\text{cap}}_{i,\phi,t}$ and the active power output of PV inverter $p^{\text{g}}_{i,\phi,t}$. Based on IEEE 1547-2018 Standard [33], the PV inverters can provide reactive power injection or absorption $q^{\text{g}}_{i,\phi,t}$ to achieve fast voltage regulation. In this work, we focus on proposing a CVR model by optimally controlling the injection or absorption of reactive power in the PV inverters against the uncertainties of loads and renewable generations. While the dispatches of the on-load tap changers

(OLTCs) and the capacitor banks (CBs) are slow and limited by a certain number of switching operations, which cannot respond to the uncertainties of loads and renewable generations. To consider the impacts of those conventional voltage regulation devices on CVR performance, a hierarchical control method [4] and [34] can be easily implemented to coordinate PV inverters, OLTC and CBs from different control stages. Note that the coordination between PV inverters, OLTC, and CBs is out of the scope of this paper. In constraint (1i), the squared bus voltage magnitude $v_{i,\phi,t}$ is limited by $v_{\min}$ and $v_{\max}$, which are typically $[0.95^2, 1.05^2]$ p.u., respectively.

The deterministic VVO-CVR problem (1) has an underlying assumption that the load and PV generation predictions are perfect, which means $t^{\mathrm{PL}}_{i,\phi,t}$, $t^{\mathrm{QL}}_{i,\phi,t}$ in constraints (1e) and (1f), and $p^{\mathrm{g}}_{i,\phi,t}$ in constraint (1h) are predefined constant parameters. The more realistic setting is to take the load and PV generation prediction errors into account. To do this, we can replace the deterministic parameters $t^{\mathrm{PL}}_{i,\phi,t}$, $t^{\mathrm{QL}}_{i,\phi,t}$, $p^{\mathrm{g}}_{i,\phi,t}$ by uncertainty variables. Particularly, we introduce two uncertainty variables $t^{\mathrm{PL},\xi}_{i,\phi,t}$ and $t^{\mathrm{QL},\xi}_{i,\phi,t}$ to replace deterministic load shape multipliers $t^{\mathrm{PL}}_{i,\phi,t}$ and $t^{\mathrm{QL}}_{i,\phi,t}$, as shown in (2a) and (2b). We reserve the super-script ξ to define the random variables, which also apply to the rest of the definition below. Then, we introduce an auxiliary variables $\alpha^{\mathrm{q}}_{i,\phi,t} \in [-1, 1]$, which represents the ratio between reactive power output $q^{\mathrm{g}}_{i,\phi,t}$ and reactive power capacity. Here, we use $Q^{\mathrm{cap},\xi}_{i,\phi,t}$ to represent the square root term $\sqrt{(S^{\mathrm{cap}}_{i,\phi,t})^2 - (p^{\mathrm{g},\xi}_{i,\phi,t})^2}$, so that the constraint (1h) can be reformulated as constraint (2c).

$$p^{\mathrm{ZIP}}_{i,\phi,t} = t^{\mathrm{PL},\xi}_{i,\phi,t} \odot \left(k^{p}_{i,1} \cdot v_{i,\phi,t} + k^{p}_{i,2} \cdot \sqrt{v_{i,\phi,t}} + k^{p}_{i,3}\right), \quad (2a)$$

$$q^{\mathrm{ZIP}}_{i,\phi,t} = t^{\mathrm{QL},\xi}_{i,\phi,t} \odot \left(k^{q}_{i,1} \cdot v_{i,\phi,t} + k^{q}_{i,2} \cdot \sqrt{v_{i,\phi,t}} + k^{q}_{i,3}\right), \quad (2b)$$

$$q^{\mathrm{g}}_{i,\phi,t} = \alpha^{\mathrm{q}}_{i,\phi,t} Q^{\mathrm{cap},\xi}_{i,\phi,t}, \forall i \in \mathcal{G}. \quad (2c)$$

We can define a uncertainty variable vector $\xi_{i,\phi,t} = [(t^{\mathrm{PL},\xi}_{i,\phi,t})^\top, (t^{\mathrm{QL},\xi}_{i,\phi,t})^\top, (p^{\mathrm{g},\xi}_{i,\phi,t})^\top, (Q^{\mathrm{cap},\xi}_{i,\phi,t})^\top]^\top$ to include all the uncertainty variables. To be simplified, we avoid the indices of i, ϕ, t in vector ξ. To consider the impacts of uncertainty ξ on voltage regulation performance, we can extend the deterministic maximum/minimum voltage constraint (1i) to two chance constraints (3a) and (3b) as follows:

$$\mathbb{P}\{v_{i,\phi,t} - v_{\max} \le 0\} \ge 1 - \epsilon \quad (3a)$$

$$\mathbb{P}\{-v_{i,\phi,t} + v_{\min} \le 0\} \ge 1 - \epsilon. \quad (3b)$$

where ϵ is a pre-defined risk level of failing to satisfy bus voltage constraint against uncertainties in ξ. To further make the solution robust to a group of probability distributions with controllable conservativeness, we introduce DRO and an ambiguity set of uncertainty to chance-constrained CVR and compactly formulate a DRCC-CVR problem (4a)-(4c) [35], [36], as follows:

$$\min_{x} \max_{\xi \sim \mathbb{P} \in \mathcal{P}} E_{\mathbb{P}}\{f(x, \xi)\}, \quad (4a)$$

$$\text{s.t. } g_1(x) \le 0, \quad (4b)$$

$$\mathbb{P}\{g_2(x, \xi) \le 0\} \ge 1 - \epsilon, \quad (4c)$$

where the max function indicates that the decisions are robust to the worst-case distribution with the ambiguity set, x represents the decision variable vector (i.e. reactive power dispatch of PV inverter), and $\xi \sim \mathbb{P} \in \mathcal{P}$ in objective (4a) means that the uncertainty variable vector ξ following the distribution $\mathbb{P}$ within an ambiguity set of distributions $\mathcal{P}$. Constraints (1b)-(1h) can be represented by the compact constraint (4b) and the chance constraints (3a) and (3b) can be represented by the compact constraint (4c).

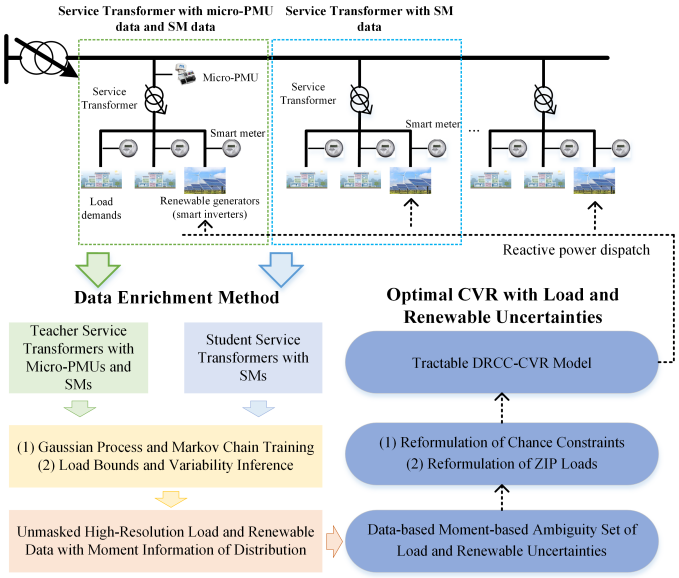

Fig. 1. Overall framework of the tractable DRCC-CVR with data enrichment method and enriched data-based moment-based ambiguity set.

B. Our Proposed Method

The challenges of solving this DRCC-CVR problem (4a)-(4c) can be summarized as follows: (i) the nonlinear power flow model and voltage-dependent ZIP load model, and the chance constraints with the random variables make the DRCC-CVR problem (4a)-(4c) intractable to be solved; and (ii) even though we can reformulate the DRCC problem in a tractable way, the limited access to the high-resolution load and PV data will lead to an ill-posed DRCC-CVR problem and hinder the performance of CVR implementation. To address those challenges, we propose a solution to address these challenges, as shown in Fig. 1, which includes the following two parts:

1) *Tractable DRCC-CVR model:* To reformulate a tractable DRCC-CVR model, we leverage the linearized Distflow model [3] and linearized voltage-dependent ZIP load model with Binominal Approximation method [31]. Then, we reformulate the chance constraints of voltage by a tractable DRCC model with a moment-based ambiguity set. Compared to other types of DRO, the DRCC with a moment-based ambiguity set has higher computational efficiency for tractable reformulation. We will show the linearized version of the power flow model and voltage-dependent ZIP load model, as well as the tractable reformulation of the DRCC-CVR problem in Section IV.

2) *Data enrichment method and moment-based Ambiguity set:* As shown in Fig. 1, there are a large number of service

transformers that can collect low-resolution load and PV generation data by SMs, while only a few service transformers are installed with micro-PMUs with access to high-resolution load and PV generation data. To capture the uncertainty of load and PV generation, we use SMs and micro-PMUs to collect load and PV generation data. Then we enrich the load and PV generation data and extract the corresponding moment information of probability distributions from the enriched load and PV data. Finally, we can construct the ambiguity set with the first two moment information i.e., mean and variance, and implement the ambiguity set in our proposed DRCC-CVR model. The purpose of introducing the data enrichment method in a data-based ambiguity set is to avoid potential over- or under-conservativeness. We will show the data enrichment method and the construction of a moment-based ambiguity set for DRCC-CVR in Section V.

IV. Tractable Reformulation of DRCC-CVR Model

This section presents the linearized version of the power flow model and voltage-dependent ZIP load model and reformulates a tractable version of the DDCC-CVR problem.

A. Linearized Reformulation of Power Flow and Voltage-Dependent ZIP Loads

In power flow constraints (1b)-(1d), the nonlinear terms $\varepsilon^p_{ij,\phi,t}$, $\varepsilon^p_{ij,\phi,t}$ and $\varepsilon^v_{i,\phi,t}$ make the optimization problems non-convex and NP hard. In practice, those nonlinear terms are much smaller than the linear terms in power flow constraints (1b)-(1d). Therefore, the constraints (1b)-(1d) can be reformulated as constraints (5a)-(5c) with linearized Distflow model by neglecting those nonlinear terms.

$$P_{ij,\phi,t} = \sum_{k:j\to k} P_{jk,\phi,t} - p^{\mathrm{g}}_{j,\phi,t} + p^{\mathrm{ZIP}}_{j,\phi,t}, \tag{5a}$$

$$Q_{ij,\phi,t} = \sum_{k:j\to k} Q_{jk,\phi,t} - q^{\mathrm{g}}_{j,\phi,t} + q^{\mathrm{ZIP}}_{j,\phi,t}, \tag{5b}$$

$$v_{j,\phi,t} = v_{i,\phi,t} - 2\big(\bar{r}_{ij} \odot P_{ij,\phi,t} + \bar{x}_{ij} \odot Q_{ij,\phi,t}\big). \tag{5c}$$

This linear form of DistFlow has been verified in many previous studies, such as [3]. The nonlinear term $\sqrt{v_{i,\phi,t}}$ of ZIP loads also introduces non-convexity to the problem. Because the voltage magnitudes of all buses in a distribution network stay close to 1 p.u. under normal operating conditions [3] and [4], the active and reactive ZIP loads can be linearized by Binominal Approximation Method [31]. Therefore, the squared deviation of voltage $(\Delta V)^2$ is very small, so it can be neglected. Then we have the following approximations (6) of squared voltage magnitude, as follows:

$$\begin{aligned} v &= V \odot V = (1+\Delta V) \odot (1+\Delta V) \approx 1 + 2\Delta V, \\ v &= 1 + \Delta v \approx 1 + 2\Delta V, \\ \Delta v &\approx 2\Delta V, \end{aligned} \tag{6}$$

where v and Δv are the vectors of squared voltage magnitude and the derivation from the nominal value, respectively; V and ΔV are the vectors of voltage magnitude and the derivation from the nominal value, respectively. By introducing equation (6) and $\sqrt{v} = V = (1+\Delta V)$ to equations (2a) and (2b), we have the linear approximation of voltage-dependent active and reactive ZIP loads as follows:

$$p^{\mathrm{ZIP}}_{i,\phi,t} \approx t^{\mathrm{PL},\xi}_{i,\phi,t} \odot \big((k^p_{i,1} + \frac{k^p_{i,2}}{2})v_{i,\phi,t} + (k^p_{i,3} + \frac{k^p_{i,2}}{2})\big), \tag{7a}$$

$$q^{\mathrm{ZIP}}_{i,\phi,t} \approx t^{\mathrm{QL},\xi}_{i,\phi,t} \odot \big((k^q_{i,1} + \frac{k^q_{i,2}}{2})v_{i,\phi,t} + (k^q_{i,3} + \frac{k^q_{i,2}}{2})\big). \tag{7b}$$

B. Tractable Reformulation of DRCC-CVR with Load and Renewable generation Uncertainties

To achieve the tractable reformulation of DRCC-CVR, the power flow constraints (1b)-(1d) can be compactly formulated as follows:

$$-AP = p, \tag{8a}$$

$$-AQ = q, \tag{8b}$$

$$-A_0 v_0 - A^\top v = -2D_r P - 2D_x Q, \tag{8c}$$

where A_0 and A are the incidence matrices of unbalanced radial distribution network, A_0 represents the connection structure between substation (the feeder head bus) and each of the line segments in $\mathcal{E}$, A represents the connection structure between the remaining buses and each of the line segment in $\mathcal{E}$. v_0 is vector of square nominal voltage magnitudes. $D_r = blkdiag[R_{bp(1)1}, ..., R_{bp(N)N}]$ and $D_x = blkdiag[X_{bp(1)1}, ..., X_{bp(N)N}]$ are block diagonal matrices of line segment resistance and reactance, respectively. In equations (8a) and (8b), the nodal active and reactive power injections can be calculated based on ZIP loads and PV generations. Based on the compact power flow formulations (8a)-(8c), we have the compact formulation (9) to represent the relationship between bus voltage v and bus power injections p and q, as follows:

$$v = Rp + Xq + \tilde{v}, \tag{9}$$

with

$$\begin{aligned} R &= 2[A^\top]^{-1} D_r A^{-1}, \\ X &= 2[A^\top]^{-1} D_r A^{-1}, \\ \tilde{v} &= -[A^\top]^{-1} A_0 v_0. \end{aligned}$$

By introducing PV inverter reactive power output equation (2c), linearized ZIP load equations (7a) and (7b) as bus power injections p and q into the compact formulation (9), we have an equation as shown in equation (10), which represents the relationship between vector of squared voltage v and all the uncertainty variables in vector ξ. Because we have the load shape multipliers $t^{PL,\xi}, t^{QL,\xi} \in [0,1]$ and the network resistance and reactance matrices R, X are also small, then the $t^{PL,\xi}\left(Rk^p_1 + R\frac{k^p_2}{2}\right)$ and $t^{QL,\xi}\left(Xk^q_1 + X\frac{k^q_2}{2}\right)$ are much smaller than identity matrix I, thus the equation (11) is valid.

$$I - t^{PL,\xi}\left(Rk^p_1 + R\frac{k^p_2}{2}\right) - t^{QL,\xi}\left(Xk^q_1 + X\frac{k^q_2}{2}\right) > 0. \tag{11}$$

After we introduce the equation (10) into the deterministic constraint (1g) on bus voltages, and because equation (11) is valid, we can obtain equation (12), which represents the impacts of load and PV generation uncertainties on bus voltage

$$v = R\left(t^{\mathrm{PL},\xi}\big((k_1^p + \frac{k_3^p}{2})v + (k_3^p + \frac{k_2^p}{2})\big) - p^{\mathrm{g},\xi}\right) + X\left(t^{\mathrm{QL},\xi}\big((k_1^q + \frac{k_3^q}{2})v + (k_3^q + \frac{k_2^q}{2})\big) - \alpha^{\mathrm{q}}Q^{\mathrm{cap},\xi}\right) + \tilde{v}, \tag{10}$$

$$v_{\min} \leq \frac{t^{\mathrm{PL},\xi}\left(Rk_3^p + R\frac{k_2^p}{2}\right) + t^{\mathrm{QL},\xi}\left(Xk_3^q + X\frac{k_2^q}{2}\right) + Rp^{\mathrm{g},\xi} + X\alpha^{\mathrm{q}}Q^{\mathrm{cap},\xi} + \tilde{v}}{I - t^{\mathrm{PL},\xi}\left(Rk_1^p + R\frac{k_2^p}{2}\right) - t^{\mathrm{QL},\xi}\left(Xk_1^q + X\frac{k_2^q}{2}\right)} \leq v_{\max}, \tag{12}$$

constraints (1i) with v_{min} and v_{max}. For simplicity, we also avoid the indices of i, ϕ, t in equations (10) and (12). The compact formulation (4c) can be reformulated in a linear form $a(x)^\top \xi + b(x) \leq 0$. We can obtain the formulations of $a(x)$ and $b(x)$ for chance constraints (3a) and (3b) by introducing the equation (12) into chance constraints (3a) and (3b). Therefore, the $a(x)$ and $b(x)$ of chance constraint (3a) can be formulated as (13a) and (13b), respectively.

$$a(x) = \begin{bmatrix} \mathrm{diag}(v_{\max})\left(Rk_1^p + R\frac{k_2^p}{2}\right) + \left(Rk_3^p + R\frac{k_2^p}{2}\right) \\ \mathrm{diag}(v_{\max})\left(Xk_1^q + X\frac{k_2^q}{2}\right) + \left(Xk_3^q + X\frac{k_2^q}{2}\right) \\ -R \\ -Xa_j \end{bmatrix}, \tag{13a}$$

$$b(x) = \tilde{v} - v_{\max}. \tag{13b}$$

Similarly, the $a(x)$ and $b(x)$ for another chance constraint (3b) can be formulated as (14a) and (14b), respectively.

$$a(x) = \begin{bmatrix} -\mathrm{diag}(v_{\min})\left(Rk_1^p + R\frac{k_2^p}{2}\right) - \left(Rk_3^p + R\frac{k_2^p}{2}\right) \\ -\mathrm{diag}(v_{\min})\left(Xk_1^q + X\frac{k_2^q}{2}\right) - \left(Xk_3^q + X\frac{k_2^q}{2}\right) \\ R \\ Xa_j \end{bmatrix}, \tag{14a}$$

$$b(x) = -\tilde{v} + v_{\min}. \tag{14b}$$

A moment-based ambiguity set of load and PV generation uncertainties can be constructed in (15), as follows:

$$\mathcal{D}_\xi = \left\{\xi \sim \mathbb{P} \in \mathcal{P} : \mathbb{E}_{\mathbb{P}_\xi}[\xi] = \mu, \mathbb{E}_{\mathbb{P}_\xi}[\xi\xi^T] = \Sigma\right\} \tag{15}$$

where μ and Σ represent the mean and covariance of the uncertain variables of load and PV generation. Finally, based on equations (13a)-(14b) for $a(x)$ and $b(x)$, we can obtain a second-order conic reformulation (16) for the DRCC (3a) and (3b) with moment information, mean μ and covariance Σ of uncertainty variable vector ξ [35] and [37], as follows: :

$$a(x)^\top \mu + b(x) + \sqrt{\frac{1-\epsilon}{\epsilon}}||\Sigma^{\frac{1}{2}} a(x)||_2 \leq 0. \tag{16}$$

Even though the mean μ and covariance Σ of load and PV generation in (16) can be extracted from recorded data of SMs and micro-PMUs, the reality is that we only have limited access to high-resolution load and PV generation data. The limited data will lead to the potential ill-posed of DRCC (16), and further hinder the performance of DRCC-CVR. Therefore, we introduce a data enrichment method for high-resolution data recovery and ambiguity set construction in Section V.

V. Data Enrichment Method And Moment-Based Ambiguity Set

This section presents the data enrichment method to recover high-resolution data of load/PV for those service transformers with only SMs. Then, the ambiguity set with moment information of probability distributions is constructed based on the enriched load/PV data. Note that even though the equations in Section V-A only contain the symbol P, the data enrichment method is applied for both active and reactive load demand powers and active PV generation power. In this section, the term *load/PV* refers to active/reactive load demand/active PV generation.

A. Data Enrichment Method with Micro-PMU and SM Data

As shown in Fig. 1, the majority of service transformers are only installed with SMs to record low-resolution load/PV data, and only a few service transformers are installed with micro-PMUs to record high-resolution data. The transformers that only have SMs can provide utilities with relatively low-resolution data. In contrast, the transformers with micro-PMUs can provide utilities with high-resolution data. The purpose of data enrichment in this section is to probabilistically decompose the low-resolution data into high-resolution data by utilizing the models learned from high-resolution data. To enrich the data of load/PV, we consider the service transformers with micro-PMU data as a teacher repository and the service transformers with only SM data as a student repository. Note that the high-resolution measurements are discretized in this data enrichment method to train the Markov Chain (MC) models for statistically learning the transition of load/PV. Discretizing includes two steps: First, the range between the maximum and the minimum boundaries of data is evenly divided into multiple contiguous bins (or intervals). Second, the high-resolution analog measurements are discretized by dividing the measurements by the bin width, and the integer part of the quotient is selected as the state for the MC model.

The entire enrichment procedure can be divided into two stages, the training stage and the teaching stage. In the training stage, the teacher service transformers train two models capturing the statistical relationship between high-resolution load/PV data and low-resolution load/PV data. In the teaching stage, the trained models of teacher transformers are then utilized to perform data enrichment for those student service transformers with only SMs. The training and teaching stages both have two steps, which are presented as follows:

Step. I *Train the load/PV generation data maximum and minimum boundary inference models:* The first step is to

train probabilistic models using the available high-resolution load/PV data from teacher service transformers with micro-PMUs. As discussed earlier, micro-PMUs can record high-resolution data. Therefore, the average power with a low resolution (e.g., an hourly power measurement) corresponds to a high-resolution time series. For a time series within a particular period, there exists one average, one maximum, and one minimum. According to real data, the maximum/minimum can be much different from the average due to the uncertainty of instantaneous load/PV. The Gaussian Process Regression (GPR) technique [32] is used to capture the relationship between the maximum/minimum bounds and the average values for load/PV. More specifically, two GPR models $GPR^*_{s,1}$ and $GPR^*_{s,2}$ are trained for the s-th teacher service transformer:

$$GPR^*_{s,1} : P_a(t) \rightarrow \overline{P}(t), \tag{17a}$$

$$GPR^*_{s,2} : P_a(t) \rightarrow \underline{P}(t), \tag{17b}$$

where $P_a(t)$ denotes the average load/PV over the t-th hour, $\overline{P}(t)$ and $\underline{P}(t)$ denote the upper and lower bounds of instantaneous load/PV within the t-th hour, respectively. These two trained models can infer the upper and lower bounds given a known average load/PV for those service transformers that only have SMs.

Step. II *Train the load/PV generation variability inference models:* The second step is to model the probabilistic transition of instantaneous load/PV within their maximum and minimum bounds using the second-order MC model. The reason for selecting the MC model is that according to real high-resolution data, the variability demonstrates the characteristics of the Markov process. Specifically, one MC model MC^*_s is trained for each service transformer:

$$MC^*_s : \{P_t(m-2), P_t(m-1)\} \rightarrow P_r(P_t(m)), \tag{18}$$

where $P_t(m-2)$, $P_t(m-1)$, and $P_t(m)$ denote the $(m-2)$-th, $(m-1)$-th, and m-th high-resolution load or PV generation samples within the t-th hour. Formulation (18) outputs the probability of $P_t(m)$ based on $P_t(m-2)$ and $P_t(m-1)$. Note that Step. I and II build the load/PV data boundary inference models and the load/PV data variability inference models with a small number of high-resolution micro-PMU data of teacher service transformers. The trained MC models can probabilistically infer the variability of instantaneous load/PV within the inferred bounds from Step I. Steps. III and IV will extend the trained load/PV probabilistic models to service transformers with only SMs, so it recovers the high-resolution load/PV data masked by the low-resolution load/PV data.

Step. III *Determine the learning weights of student service transformers with respect to teacher service transformers:* The third step evaluates the low-resolution data similarity between the teacher with micro-PMUs and student service transformers with SMs by determining the learning weights as shown in (19a) and in (19b), respectively. The weights W_s and W'_s can represent the confidence of a student service transformer to learn from multiple teacher service transformers for enriching the low-resolution data to high-resolution data. Intuitively, for example, the high-resolution load data of a service transformer with a larger number of customers is less volatile than a service transformer supplying a relatively smaller number of customers. The weights are computed as follows:

$$W_s = \frac{W'_s}{\sum_{s=1}^{N_t} W'_s}, \tag{19a}$$

$$W'_s = \frac{1}{N_c N_c^s} \sum_{i=1}^{N_c} \sum_{j=1}^{N_c^s} ||P_i - P_j^s||, s = \{1, ..., N_t\}, \tag{19b}$$

where N_c and N_c^s denote the number of customers served by a student service transformer and the s-th teacher service transformer, respectively. We can obtain N_c daily load/PV patterns for that service transformer, $\{P_1, \cdots, P_{N_c}\}$. Similarly, the load/PV patterns for the s-th teacher service transformer are denoted by $\{P_1^s, \cdots, P_{N_c^s}^s\}, s = 1, \cdots, N_t$. The weights are used to linearly combine the estimated bounds in (17) and the probabilistic transition matrices in (18).

Step. IV *Extend the trained load/PV generation data probabilistic model:* The fourth step extends the trained probabilistic models of teacher service transformers in Steps. I and II to student service transformers that only have SMs for enriching low-resolution load/PV data. Specifically, the m-th high-resolution load/PV sample is randomly generated based on the following Bernoulli distribution:

$$P_t(m) \sim Be(Pr(P_t)), \tag{20}$$

where Be denotes the Bernoulli distribution [32]. Note that for each hourly load/PV sample, (20) can give us N' high-resolution samples, i.e., $P_t(m), m = 1, \cdots, N'$. Then, the enriched high-resolution data samples are employed to optimize the mean and standard deviation of Gaussian distribution using maximum likelihood estimation:

$$(\mu^*, \Sigma^*) = \underset{\mu,\Sigma}{argmin} \prod_{m=1}^{N'} f(\mu, \Sigma; P_t(m)), \tag{21}$$

where $f(\cdot)$ denotes the probability density function of Gaussian distribution. Therefore, the mean and covariance of load/PV uncertainties μ and Σ can be extracted from enriched data in (21) for the construction of the moment-based ambiguity set (15). i.e., substitute μ^* and Σ^* in (21) into (16). Note that Step-I and II learn two models that can capture the high-resolution variations based on high-resolution data of services transformers installed with micro-PMUs. Step-III and IV extend the learned models to those transformers that only have SMs for recovering the high-resolution variations hidden behind the low-resolution data. Therefore, the high-resolution variations of load/PV have already been considered in this data enrichment method.

B. Enriched Data-Based Ambiguity Set and DRCC-CVR Method

The enriched high-resolution data from (20) can recover instantaneous uncertainties of load/PV, which can be further extracted for the two moment information and construct moment-based ambiguity set in (15). By considering the data enriched moment-based ambiguity set and the reformulation of tractable

Algorithm 1 DRCC-CVR Model with Enriched-based Ambiguity Set of Uncertainty of Load and PV Generation

1: **Input**: High-resolution data from micro-PMUs and low-resolution data from SMs
2: **Initialization**: Choose hyper-parameters in DRCC-CVR
3: **For**: $i = 1, 2, ..., N$.
4: Train load/PV upper and lower boundary inference models from teacher service transformers with micro-PMUs by (17a) and (17b).
5: Train load/PV variability inference model from teacher service transformers with micro-PMUs by (18).
6: Determine the learning weights of student service transformers with respect to teacher service transformers in (19a) and (19b).
7: Extend the trained load/PV data to student service transformers with SMs in (20).
8: **End for**.
9: Extract the first two moment information of load/PV uncertainties from enriched data in (21)
10: Construct an ambiguity set with the first two moment information in (15).
11: Solve the DRCC-CVR problem (22) with the objective function (1) and the constraints (2c),(5),(7), (13)-(14), and (16).
12: **Output**: Reactive power dispatches of PV inverters

DRO and chance constraints, the DRCC-CVR problem can be compactly reformulated as follows:

$$\text{Objective} \quad \sup_{\xi \in \mathcal{D}_\xi} (1), \tag{22a}$$

$$\text{s.t. PV generations } \{(2c)\}, \tag{22b}$$

$$\text{OPF constraints } \{(5)\}, \tag{22c}$$

$$\text{Linearized ZIP loads } \{(7)\}, \tag{22d}$$

$$\text{Tractable reformulation of DRCC } \{(13)-(14), (16)\}. \tag{22e}$$

Note that problem (22) is a tractable problem with linear constraints (22b)-(22d) and second-order constraint (22e), where the mean values of load and PV are used in compact constraints (22b)-(22d) and the mean and covariance values of load/PV are used in the compact constraint (22e) of DRCC reformulation. To summarize the above steps, the detailed procedure of the proposed DRCC-CVR with an enriched-based ambiguity set of the uncertainties of load/PV is shown in Algorithm 1.

VI. Case Studies

This section presents the simulation results, including the enriched data of load/PV for ambiguity set, comparison results of the benchmark methods and the proposed DRCC-CVR method, and the impacts of hyper-parameter on the proposed DRCC-CVR method.

A. Simulation Setup

A real-world distribution feeder [38] in Fig. 2 is used to test our proposed DRCC-CVR method, which is located in

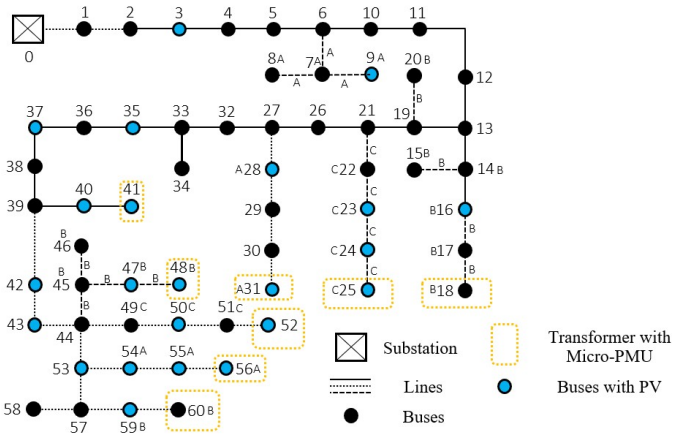

Fig. 2. A real distribution feeder in Midwest U.S. [38]

Midwest U.S. and shared by our utility partner. The reason for choosing this real-world distribution feeder as our test system is that the service transformers of customers in this feeder are either equipped with SMs or micro-PMUs, which can record low-resolution (1-hour) data and high-resolution (1-second) data to construct an ambiguity set of load/PV uncertainties for our DRCC-CVR method. More information on this real-world distribution feeder and the data from SMs and micro-PMUs can be found in [38]. In Fig. 2, the yellow botted boxes represent the buses' service transformers installed with micro-PMUs, and the rest buses' service transformers are installed with SMs; the blue dots represent the buses installed with single-phase or three-phase PV generators; the solid, dashed and dotted lines represent three-phase overhead lines, three-phase underground cables and single-phase overhead lines, respectively. In this real-world distribution feeder, the total capacity of PVs can serve nearly 25% of the total load demand. Adopted from our industrial partner [4], we use the following coefficients $[k_1^p, k_2^p, k_3^p] = [0.96, -1.17, 1.21]$ and $[k_1^q, k_2^q, k_3^q] = [6.28, -10.16, 4.88]$ for active and reactive ZIP loads in our test cases. Because most of the customers in this real-world distribution feeder [38] are residential loads. Therefore, we use those ZIP coefficients for all loads in the following simulation cases. The base voltage and base power values are 13.8 kV and 100 kVA, respectively. The prescribed risk level parameter ϵ is set to 0.05 for quantifying the 5% violation probability of chance constraints in our proposed DRCC-CVR model. We demonstrate the advantages and effectiveness of the enriched data-based ambiguity set and the proposed DRCC-CVR method through numerical comparisons of several benchmark methods. The following simulations are built-in MATLAB R2019b, which integrates YALMIP Toolbox with IBM ILOG CPLEX 12.9 solver for optimization. All case studies are simulated on a PC with Intel Core i7-4790 3.6 GHz CPU and 16 GB RAM.

This article has been accepted for publication in IEEE Transactions on Power Systems. This is the author's version which has not been fully edited and content may change prior to final publication. Citation information: DOI 10.1109/TPWRS.2023.3244895

B. The proposed data enrichment method and benchmark data enrichment methods

We have compared our proposed data enrichment method with two benchmark data enrichment methods: the method of adding random noise to typical or known load profiles [39] and the allocation-based method [40]. For conciseness, we refer to the method presented in [39] as the noise-based method. The basic idea of the noise-based method is adding random noise to a low-resolution load measurement for generating multiple high-resolution load samples. For the allocation-based method, there are two primary steps [40]. First, a low-resolution substation- or feeder-level load profile is scaled to obtain service transformer-level load profiles, according to transformer capacity or peak load. Then, the scaled low-resolution load profile is enriched using a variability library, which is constructed by applying the discrete wavelet transform algorithm to known high-resolution transformer-level load measurements. An alternative of the foregoing scaled low-resolution load profile is a load pattern obtained by scaling typical load profiles of other transformers, as presented in [40]. The performance of the noise-based method, allocation-based method, and our method is shown in Fig. 3(a), Fig. 3(b), and Fig. 3(c), respectively, where the actual and enriched load curves on a certain day are presented. We can observe that the allocation-based load enrichment method cannot accurately track the basic load pattern, as demonstrated in Fig. 3(b). The reason is that the low-resolution load curve derived from the substation, feeder, or other transformers, might not match the actual load profile of a particular service transformer because each transformer can have a distinct load signature. Fig. 3(a) shows the actual high-resolution load curve and the noise-based load curve obtained by adding Gaussian noise to a known low-resolution load profile. One primary shortcoming of the noise-based method is that it cannot capture the cyclicity of the load state, i.e., the enriched load curve clutters the plot and does not present a clear switching between different load states. In contrast, in Fig. 3(c), we can observe that the basic pattern of the enriched high-resolution load obtained from our proposed data enrichment method can flexibly follow the actual load variation, despite load uncertainty. The superior performance of our method results from two aspects: the fine spatial granularity of smart meter data and the design of the load boundary inference process.

The performances of the noise-based method and allocation-based method can also be evaluated by examining the computed R^2 values, as shown in Fig. 4 and Fig. 5. We can observe that the R^2 values are negative, which means that the estimated maximum/minimum bound offers a poor explanation for the variations of the actual maximum/minimum bound. The unsatisfying performance of the allocation-based method can also be viewed by observing the two scatter plots in Fig. 5, where most data points are located above the upper-right diagonal line, which means an overestimation of the actual load bounds. Note that the scatter plots contain all the hourly maximum/minimum loads over the entire time period of the dataset, not only the loads during a particular day. This is because one day only has 24 scatters, which is insufficient for

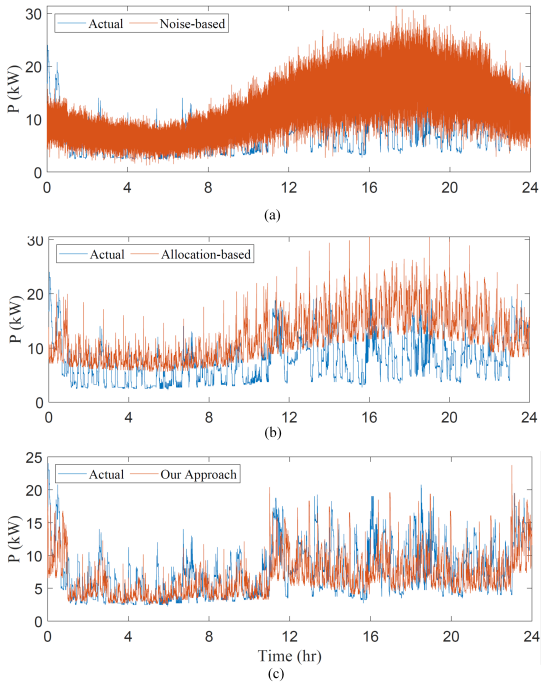

Fig. 3. The actual high-resolution load curve and the enriched load curves: (a) The actual curve and the enriched curve obtained using the noise-based method; (b) The actual curve and the enriched curve obtained using the allocation-based method; (c) The actual curve and the enriched curve obtained using our method.

creating a comprehensive scatter plot. In contrast, the two R^2 values obtained from our method are 0.80 and 0.83, which demonstrates the accuracy of our method. To further evaluate the performances of our method and the other two methods, we have also computed the cumulative probability of the actual and enriched load presented in Fig. 3. The empirical cumulative distribution functions (ECDFs) are illustrated in Fig. 6, where we can observe that the ECDF corresponding to our method is much closer to the ECDF of the actual load than the ECDFs corresponding to the allocation-based and the noise-based methods. To quantitatively assess the similarity between two ECDFs, we have computed the two-sample Kolmogorov-Smirnov (KS) statistic for each method, as follows:

$$D = \sup_{P} |F_a(P) - F_e(P)|, \tag{23}$$

where sup denotes the supremum of the set of distances. $F_a(P)$ denotes the ECDF of the actual high-resolution load, and $F_e(P)$denotes the ECDF of the enriched load. Intuitively, D measures the largest pairwise absolute distance between the ECDFs of the actual load and the enriched load. In Fig. 6, we can observe that the two-sample KS statistic for our method is 0.14, which is significantly smaller than the statistic for the allocation-based method and the noise-based method, i.e., 0.40 and 0.32, respectively.

C. Original and Enriched Data of Load and PV Generation

As shown in Fig. 2, there are 8 service transformers installed with micro-PMUs and the rest 34 service transformers installed with SMs, which can record high-resolution (1-

This article has been accepted for publication in IEEE Transactions on Power Systems. This is the author's version which has not been fully edited and content may change prior to final publication. Citation information: DOI 10.1109/TPWRS.2023.3244895

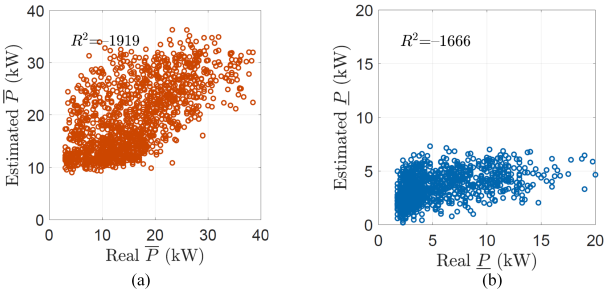

Fig. 4. The load bounds obtained from the noise-based method against the corresponding actual values: (a) Maximum; (b) Minimum.

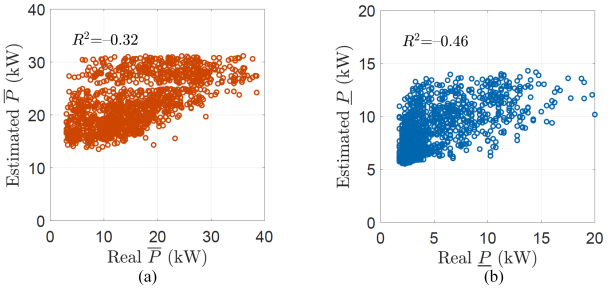

Fig. 5. The load bounds obtained from the allocation-based method against the corresponding actual values: (a) Maximum; (b) Minimum.

second) and low-resolution (1-hour) load and PV generation data, respectively. In this sub-section, we use two ways to obtain the mean and covariance of the uncertainty variables of load and PV generation for ambiguity sets: (i) we use a statistical method to obtain mean and variance information of the original load and PV generation data (few high-resolution data from 8 micro-PMUs and a lot of low-resolution data from 34 SMs). (ii) We use the data enrichment method to enrich the original load and PV generation data, then obtain mean and variance information of the enriched data. To verify the effeteness of the data enrichment method, we show the empirical distributions and their according fitted Gaussian distributions of active load, reactive load, and active power output of PV generation at 20:00 PM as examples, in Fig. 7 and Fig. 8, respectively. Note that the distributions in the right column and left column of Fig. 7 and Fig. 8 are obtained from original high-resolution data and enriched data, respectively. In our dataset, we know the original low-resolution data recorded

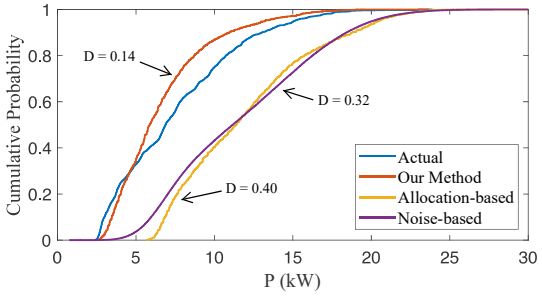

Fig. 6. Cumulative probability distributions of the actual load and the enriched load.

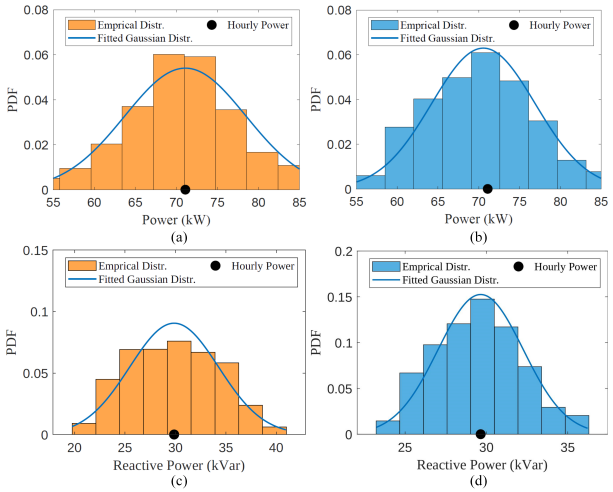

Fig. 7. Empirical distribution and fitted Gaussian distribution: (a) active load (original high-solution data); (b) active load (enriched data); (c) reactive load (original high-solution data); (d) reactive load (enriched data).

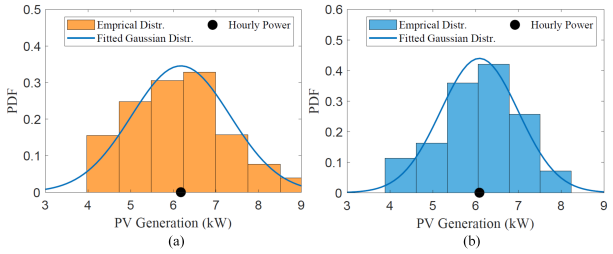

Fig. 8. Empirical distribution and fitted Gaussian distribution: (a) PV generation (original high-solution data); (b) PV generation (enriched data).

by SMs, and we also know the original high-resolution data recorded by metering devices installed by the utility for the purpose of validation. Note that in practice, only those service transformers with micro-PMUs have known high-resolution data. Therefore, the original high-resolution data is not known in practice if no extra metering devices are installed for validation. In addition, our approach can provide us with enriched high-resolution data by decomposing low-resolution SM data. In Fig. 7 and Fig. 8, each dot denotes the hourly average power corresponding to the data samples, which means the hourly power is the average of observations. It can be observed that the distributions obtained from enriched data have a highly similar fitting to the distributions obtained from original data.

To quantitatively evaluate the difference between the fitted Gaussian distributions from original high-resolution data and from the enriched data, we have computed the mean and standard deviation for those two types of data. We have also considered the mean from the original low-resolution data. We select the active load power at 20:00 PM as an example, as shown in Table I. We can observe that, due to the low (hourly) time resolution, the variance of active load cannot be obtained from original low-resolution data, which cannot capture the uncertainty of data. The differences between the original high-resolution data and the enriched data in terms of mean and

TABLE I
COMPARISON OF FIRST TWO MOMENT INFORMATION BETWEEN DIFFERENT DATA SETS.

First two moment information	Original low-resolution data	Original high-resolution data	Enriched data
Mean (kW)	73.0094	71.0915	70.5611
Standard deviation (kW)	-	7.3839	6.3381

standard deviation are small, which demonstrates the satisfying performance of our approach. Therefore, the first two moment information extracted from enriched data can also accurately construct the ambiguity set for the DRCC-CVR method.

D. Voltage Reduction and Power/energy-saving Through CVR Implementation

To serve as a reference to investigate the performance of VVO-CVR, a base case is first built by setting the unity-power factor control model for all PV generators, which means there is no reactive power support from PV generators. In this subsection, we use two ways to implement VVO-CVR: (i) The robust VVO-CVR (RO-CVR) is solved by the robust optimization [7] and [8], where the uncertainties of load and PV generation are considered with 10% variance from the predictions. (ii) The VVO-CVR is solved by our proposed DRCC-CVR with an enriched data-based ambiguity set of load and PV generation uncertainties. The performance through CVR implementation can be evaluated from three aspects: voltage profile, active power supply from the substation, and total energy consumption. To show the time-series simulation, the VVO-CVR is performed in a daily operation of the real-world distribution feeder with different control strategies. In Fig. 9, the voltage profiles for a selected bus (bus 23 on phase c) are shown, which are generated from the base case (without control) and the proposed DRCC-CVR. In Fig. 9, the blue bar and red bar represent the voltage profiles of the base case and DRCC-CVR, respectively. It can be observed that all the nodal voltages can maintain within the predefined range [0.95,1.05] p.u., while the voltage profiles of DRCC-CVR are overall lower than the voltage profiles of the base case. Because the DRCC-CVR can optimally dispatch the reactive power from PV inverters to achieve maximum voltage reduction while still satisfying the voltage constraints. During the midnight period from 00:00 to 6:00, the voltage reduction of DRCC-CVR is obviously higher than the voltage reduction of the base case, as shown in the circled part in Fig. 9. It is because the active power outputs of PV generators from 00:00 to 6:00 are nearly zero, and according to the calculations of reactive power output and capacity in constraints (1g) and equation (1h), the DRCC-CVR has more reactive power supports to maximize voltage reductions. Also, our model considers not only the uncertainties from PV generations but also the load uncertainties. At night, the load uncertainties might have more significant variations than the nighttime duration.

The active power supplies from the substation of the base case, RO-CVR, and DDRC-CVR are shown as different curves in Fig. 10, which represent the overall active power consumption of the base case and those VVO-CVR benchmarks. It can be observed that the proposed DDRC-CVR can effectively reduce the power supply from the substation compared to the base case and other methods. In comparison, the power saving of RO-CVR is less than the proposed DDRC-CVR. On the one hand, the proposed DDRC-CVR has an ambiguity set of uncertainties to balance the tradeoff between the conservativeness of decisions and operational efficiency. The numerical comparisons of total energy consumption over one day and the energy reduction percentage are presented in Table II among base case, RO-CVR, and DDRC-CVR. The total energy consumption of base case, RO-CVR, and DRCC-CVR are 958.045 kWh, 934.178 kWh, and 898.616 kWh, respectively. Therefore, compared to the original energy consumption in the base case, the energy savings of RO-CVR and DRCC-CVR can achieve 2.491% and 6.203%, respectively. The computational times of RO-CVR and DRCC-CVR for this test system are 18.312 seconds and 21.911 seconds, respectively.

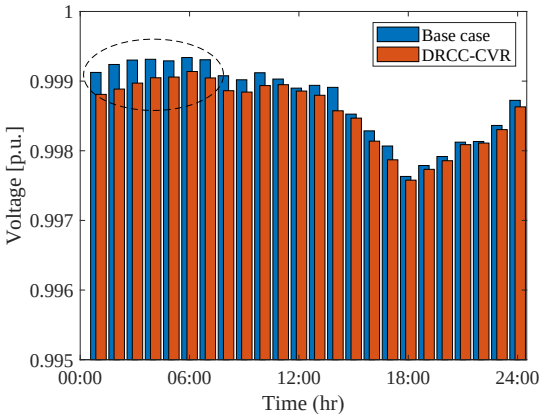

Fig. 9. Voltage profiles on selected bus 23 on phase c with different control strategies.

According to the above results in Fig. 9, Fig. 10 and Table II, we can summarize the differences between RO-CVR and DRCC-CVR: (i) Compared to 934.178 kWh and 2.491% of RO-CVR, DRCC-CVR can achieve the lower total energy consumption 898.616 kWh and higher energy saving 6.203%. On the one hand, RO-CVR is too conservative and hinders the performance of CVR implementation. On the other hand, the proposed DDRC-CVR can better explore the potential of CVR implementation. (ii) Because of the different ways of handling uncertainties of load and PV generation, the computation time 21.911 seconds of DRCC-CVR is slightly slower than the computation time 18.312 seconds of RO-CVR. However, their differences in computational time are very small, which can be neglected for a day-ahead operational application. Thus the computational efficiency of the DRCC-CVR can be acceptable. Note that no matter the timescale of DRCC-CVR is long or short, it will not make the distributions in the data enrichment stationary or causes any communication issue. As shown in the pseudo-code Algorithm 1, the high-resolution data from micro-PMU and low-resolution data from SMs are transferred into the data enrichment method (row 3 to row 8), then the first two moment information of load and PV uncer-

This article has been accepted for publication in IEEE Transactions on Power Systems. This is the author's version which has not been fully edited and content may change prior to final publication. Citation information: DOI 10.1109/TPWRS.2023.3244895

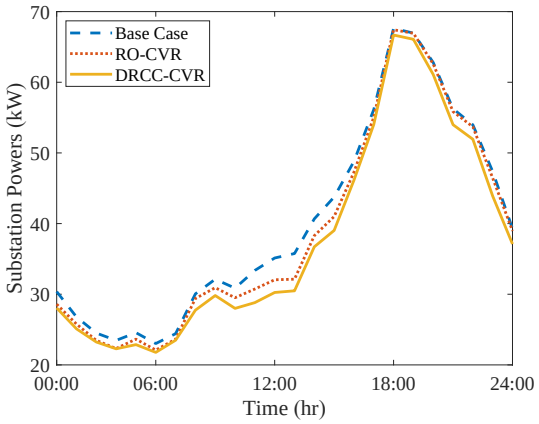

Fig. 10. Substation feed-in active power with different control strategies.

TABLE II
ENERGY CONSUMPTION AND ENERGY-SAVING RESULTS WITH DIFFERENT CONTROL STRATEGIES

	Energy (kWh)	Reduction (%)	Computation (sec)
Base Case	958.045	-	-
RO-CVR	934.178	2.491%	18.312
DRCC-CVR	898.616	6.203%	21.911

tainties are extracted from the enriched data (row 9) and the ambiguity set can be constructed by the first two moment information (row 10). Finally, the DRCC-CVR with ambiguity set is solved (row 11). Even though the mean and covariance trajectories from the data enrichment method are received by the DRCC-CVR formulation, the results from the DRCC-CVR formulation are not feedbacked to the data enrichment method.

E. Impact of Hyper-Parameters in Performance of DRCC-CVR

It is clear that a larger number of micro-PMUs can capture more high-resolution variations of load demands and PV generation. To further demonstrate the advantage of having micro-PMU measurements with a data-enriched process, we show a comparison study under different numbers of micro-PMUs using the proposed DRCC-CVR algorithm, whose results are given in Table III. There are three different tests: the first test only constructs the ambiguity set based on low-resolution data from SMs without any high-resolution data from micro-PMU; the second test implements the data enrichment method with high-resolution data from 4 micro-PMUs and low-resolution data from SMs, then the ambiguity set is constructed based on the enriched data; the third test has the high-resolution data from 8 micro-PMUs as the same setting in Section V-B and Section V-C. The case having high-resolution data as inputs to construct the ambiguity sets eventually achieves a better performance of CVR implementation through DRCC-CVR.

The pre-defined risk level ϵ is selected as 0.05 in the above simulation tests. While the different values of ϵ will influence the confidence level on chance constraints in the proposed DRCC-CVR and further influence the benefits of CVR implementation. Therefore, we also test the DRCC-CVR with three different violation rates (i.e. 0.02, 0.05, 0.1), as shown in Table IV. It can be observed that a larger value of ϵ leads to lower energy consumption and a higher energy reduction, which will benefit the CVR implementation. However, this kind of benefit is achieved by increasing the violation rate and sacrificing the reliability of operational constraints. For example, the energy reduction (6.606%) of $\epsilon = 0.1$ is only slightly higher than the energy reduction (6.203%) with $\epsilon = 0.1$. However, when the violation rate ϵ increases from 0.05 to 0.1, theoretically, the risk of constraint violation will also become higher. The results indicate that there is a tradeoff between the maximization of CVR benefit and the reliability of operational constraints in the proposed DRCC-CVR.

TABLE III
ENERGY CONSUMPTION AND ENERGY-SAVING RESULTS WITH DIFFERENT NUMBER OF MICRO-PMUS.

Number of micro-PMUs	Location of micro-PMUs	Energy (kWh)	Saving (%)
0 (only SM data)	-	933.889	2.521%
4	$B_{18}, B_{25}, B_{41}, B_{60}$	927.817	3.155%
8	$B_{18}, B_{25}, B_{31}, B_{41}$ $B_{48}, B_{52}, B_{56}, B_{60}$	898.618	6.203%

TABLE IV
ENERGY CONSUMPTION AND ENERGY-SAVING RESULTS WITH DIFFERENT VIOLATION RATES.

	Energy (kWh)	Reduction (%)
$\epsilon = 0.02$	904.980	4.803%
$\epsilon = 0.05$	898.616	6.203%
$\epsilon = 0.1$	894.754	6.606%

VII. CONCLUSION

To better consider the impacts of load and PV generation uncertainties on voltage regulating performance while implementing CVR in unbalanced three-phase distribution systems, a DRCC-CVR model with an enriched data-based and moment-based ambiguity set is proposed to optimally dispatch the reactive power of PV inverters. The original and intractable DRCC-CVR is approximated by linearized ZIP load models and reformulated in a tractable way with the first two moment information of load and PV generation uncertainties. We further implement a data enrichment method with low-resolution data from SMs and high-resolution data from micro-PMUs to recover instantaneous uncertainties of load and PV generation. An ambiguity set is constructed based on enriched data for DRCC-CVR. Simulation results on a real Midwest U.S. distribution feeder have validated the effectiveness and robustness of the proposed DRCC-CVR. According to the case studies, we have shown that: (i) The data enrichment can construct an accurate ambiguity set of load and PV generation uncertainties. (ii) Compared to 2.491% energy saving of RO-CVR, the proposed DRCC-CVR can reach a higher 6.203% energy saving, which means the proposed DRCC-CVR can achieve

better CVR performance and show a better tradeoff between the conservativeness of decisions and operational efficiency. (iii) By comparing different numbers (0, 4, and 8) of micro-PMUs in the data enrichment method, it can be observed that a high-quality ambiguity set can be constructed with a higher number of micro-PMUs for DRCC-CVR and better performance of CVR can be achieved. (iv) By increasing the confidence level from 0.02 to 0.1, the total energy consumption and energy saving change from 904.98 kWh to 894.754 kWh and 4.803% to 6.606%. Theoretically, the risk of constraint violation will become higher with a larger value of confidence level. Therefore, a proper risk and confidence level needs to be tuned in DRCC- to consider the tradeoff between CVR implementation and the reliability of operational constraints.

A certain level of temporal and spatial correlation of loads and PVs has been considered by the moment information in our data enrichment method and DRCC-CVR method. Our proposed DRCC-CVR method is implemented in the primary distribution network, which means the loads and PV generations in the secondary distribution networks have been aggregated into the nodal level of the primary distribution network. Even though a moment-based approach with a data enrichment method is good enough to consider the temporal and spatial correlation of load and PV uncertainties and implement DRCC-CVR in the primary distribution network. Future work still needs to be done for further consideration of the temporal and spatial correlations of load and PV generation uncertainties. The smart meter and micro-PMU data can be better utilized by exploring other alternatives to construct an uncertainty set and implement the DRCC-CVR method, e.g., by using a minimum volume enclosing convex hull uncertainty set [41] or f-divergence ambiguity set [42] instead of a moment-based ambiguity set.

REFERENCES

[1] Z. Wang and J. Wang, "Review on implementation and assessment of conservation voltage reduction," *IEEE Trans. Power Syst.*, vol. 29, no. 3, pp. 1306–1315, 2014.

[2] T. V. Dao, S. Chaitusaney, and H. T. N. Nguyen, "Linear least-squares method for conservation voltage reduction in distribution systems with photovoltaic inverters," *IEEE Trans. Smart Grid*, vol. 8, no. 3, pp. 1252–1263, 2017.

[3] Q. Zhang, K. Dehghanpour, and Z. Wang, "Distributed CVR in unbalanced distribution systems with PV penetration," *IEEE Trans. Smart Grid*, vol. 10, no. 5, pp. 5308–5319, Sept. 2019.

[4] Q. Zhang, Y. Guo, Z. Wang, and F. Bu, "Distributed optimal conservation voltage reduction in integrated primary-secondary distribution systems," *IEEE Trans. Smart Grid*, vol. 12, no. 5, pp. 3889–3900, 2021.

[5] J. A. Momoh, S. S. Reddy, and Y. Baxi, "Stochastic voltage/var control with load variation," in *2014 IEEE PES General Meeting (PESGM)*, 2014, pp. 1–5.

[6] A. Samimi and A. Kazemi, "Scenario-based stochastic programming for Volt/Var control in distribution systems with renewable energy sources," *IETE Technical Review*, vol. 33, no. 6, pp. 638–650, 2016.

[7] R. A. Jabr, "Robust volt/var control with photovoltaics," *IEEE Trans. Power Syst.*, vol. 34, no. 3, pp. 2401–2408, 2019.

[8] M. Azarnia and M. Rahimiyan, "Robust volt-var control of a smart distribution system under uncertain voltage-dependent load and renewable production," *Int. J. Electr. Power Energy Syst.*, vol. 134, p. 107383, 2022.

[9] Y. Chen, W. Wei, F. Liu, and S. Mei, "Distributionally robust hydro-thermal-wind economic dispatch," *Appl. Energy*, vol. 173, pp. 511–519, 2016.

[10] C. Ning and F. You, "Deep learning based distributionally robust joint chance constrained economic dispatch under wind power uncertainty," *IEEE Trans. Power Syst.*, vol. 37, no. 1, pp. 191–203, 2022.

[11] B. K. Poolla, A. R. Hota, S. Bolognani, D. S. Callaway, and A. Cherukuri, "Wasserstein distributionally robust look-ahead economic dispatch," *IEEE Trans. Power Syst.*, vol. 36, no. 3, pp. 2010–2022, 2021.

[12] Y. Yang and W. Wu, "A distributionally robust optimization model for real-time power dispatch in distribution networks," *IEEE Trans. Smart Grid*, vol. 10, no. 4, pp. 3743–3752, 2019.

[13] L. Dong, J. Li, T. Pu, and N. Chen, "Distributionally robust optimization model of active distribution network considering uncertainties of source and load," *J. Mod. Power Syst. Clean Energy*, vol. 7, no. 6, pp. 1585–1595, 2019.

[14] R. Mieth and Y. Dvorkin, "Data-driven distributionally robust optimal power flow for distribution systems," *IEEE Control Syst. Lett.*, vol. 2, no. 3, pp. 363–368, 2018.

[15] Y. Ding, T. Morstyn, and M. D. McCulloch, "Distributionally robust joint chance-constrained optimization for networked microgrids considering contingencies and renewable uncertainty," *IEEE Trans. Smart Grid*, vol. 13, no. 3, pp. 2467–2478, 2022.

[16] C. Duan, W. Fang, L. Jiang, L. Yao, and J. Liu, "Distributionally robust chance-constrained approximate ac-opf with wasserstein metric," *IEEE Trans. Power Syst.*, vol. 33, no. 5, pp. 4924–4936, 2018.

[17] R. Zhu, H. Wei, and X. Bai, "Wasserstein metric based distributionally robust approximate framework for unit commitment," *IEEE Trans. Power Syst.*, vol. 34, no. 4, pp. 2991–3001, 2019.

[18] X. Zheng and H. Chen, "Data-driven distributionally robust unit commitment with wasserstein metric: Tractable formulation and efficient solution method," *IEEE Trans. Power Syst.*, vol. 35, no. 6, pp. 4940–4943, 2020.

[19] S. Wang, C. Zhao, L. Fan, and R. Bo, "Distributionally robust unit commitment with flexible generation resources considering renewable energy uncertainty," *IEEE Trans. Power Syst.*, pp. 1–1, 2022.

[20] P. Li, C. Wang, Q. Wu, and M. Yang, "Risk-based distributionally robust real-time dispatch considering voltage security," *IEEE Trans. Sustain. Energy*, vol. 12, no. 1, pp. 36–45, 2021.

[21] J. Liu, Y. Chen, C. Duan, J. Lin, and J. Lyu, "Distributionally robust optimal reactive power dispatch with wasserstein distance in active distribution network," *J. Mod. Power Syst. Clean Energy*, vol. 8, no. 3, pp. 426–436, 2020.

[22] Z. Zhang, F. F. da Silva, Y. Guo, C. L. Bak, and Z. Chen, "Coordinated voltage control in unbalanced distribution networks with two-stage distributionally robust chance-constrained receding horizon control," *Renew. Energy*, 2022.

[23] G. Chen, H. Zhang, H. Hui, and Y. Song, "Fast wasserstein-distance-based distributionally robust chance-constrained power dispatch for multi-zone hvac systems," *IEEE Trans. Smart Grid*, vol. 12, no. 5, pp. 4016–4028, 2021.

[24] P. Mohajerin Esfahani and D. Kuhn, "Data-driven distributionally robust optimization using the wasserstein metric: Performance guarantees and tractable reformulations," *Math. Program.*, vol. 171, no. 1, pp. 115–166, 2018.

[25] B. Li, R. Jiang, and J. L. Mathieu, "Distributionally robust chance-constrained optimal power flow assuming unimodal distributions with misspecified modes," *IEEE Trans. Control. Netw. Syst.*, vol. 6, no. 3, pp. 1223–1234, 2019.

[26] L. Yang, Y. Xu, W. Gu, and H. Sun, "Distributionally robust chance-constrained optimal power-gas flow under bidirectional interactions considering uncertain wind power," *IEEE Trans. Smart Grid*, vol. 12, no. 2, pp. 1722–1735, 2021.

[27] Y. Guo, K. Baker, E. Dall'Anese, Z. Hu, and T. H. Summers, "Data-based distributionally robust stochastic optimal power flow—part I: Methodologies," *IEEE Trans. Power Syst.*, vol. 34, no. 2, pp. 1483–1492, 2019.

[28] ——, "Data-based distributionally robust stochastic optimal power flow—part II: Case studies," *IEEE Trans. Power Syst.*, vol. 34, no. 2, pp. 1493–1503, 2019.

[29] L. Yang, Y. Xu, H. Sun, and W. Wu, "Tractable convex approximations for distributionally robust joint chance constrained optimal power flow under uncertainties," *IEEE Trans. Power Syst.*, pp. 1–1, 2021.

[30] Z. Shen, Z. Wei, G. Sun, and S. Chen, "Representing ZIP loads in convex relaxations of optimal power flow problems," *Int. J. Electr. Power Energy Syst.*, vol. 110, pp. 372–385, 2019.

[31] F. U. Nazir, B. C. Pal, and R. A. Jabr, "Approximate load models for conic OPF solvers," *IEEE Trans. Power Syst.*, vol. 36, no. 1, pp. 549–552, 2021.

[32] F. Bu, K. Dehghanpour, and Z. Wang, "Enriching load data using micro-pmus and smart meters," *IEEE Trans. Smart Grid*, vol. 12, no. 6, pp. 5084–5094, 2021.

[33] "IEEE standard for interconnection and interoperability of distributed energy resources with associated electric power systems interfaces," *IEEE Std 1547-2018 (Revision of IEEE Std 1547-2003)*, pp. 1–138, 2018.

[34] R. Cheng, Z. Wang, Y. Guo, and Q. Zhang, "Online voltage control for unbalanced distribution networks using projected newton method," *IEEE Trans. Power Syst.*, pp. 1–1, 2022.

[35] E. Delage and Y. Ye, "Distributionally robust optimization under moment uncertainty with application to data-driven problems," *Oper. Res.*, vol. 58, no. 3, pp. 595–612, 2010.

[36] J. Zhai, Y. Jiang, Y. Shi, C. N. Jones, and X.-P. Zhang, "Distributionally robust joint chance-constrained dispatch for integrated transmission-distribution systems via distributed optimization," *IEEE Trans. Smart Grid*, vol. 13, no. 3, pp. 2132–2147, 2022.

[37] G. C. Calafiore and L. El Ghaoui, "On distributionally robust chance-constrained linear programs," *J Optim Theory Appl.*, vol. 130, no. 1, pp. 1–22, 2006.

[38] F. Bu, Y. Yuan, Z. Wang, K. Dehghanpour, and A. Kimber, "A time-series distribution test system based on real utility data," in *Proc. North American Power Symposium (NAPS)*, 2019, pp. 1–6.

[39] A. Ghosh, D. Lubkeman, and R. Jones, "Load modeling for distribution circuit state estimation," *IEEE Trans. Power Deliv.*, vol. 12, no. 2, pp. 999–1005, 1997.

[40] X. Zhu and B. Mather, "Data-driven distribution system load modeling for quasi-static time-series simulation," *IEEE Trans. Smart Grid*, vol. 11, no. 2, pp. 1556–1565, 2020.

[41] Y. Zhang, Y. Liu, S. Shu, F. Zheng, and Z. Huang, "A data-driven distributionally robust optimization model for multi-energy coupled system considering the temporal-spatial correlation and distribution uncertainty of renewable energy sources," *Energy*, vol. 216, p. 119171, 2021.

[42] C. Ning and F. You, "Data-driven ambiguous joint chance constrained economic dispatch with correlated wind power uncertainty," in *2021 American Control Conference (ACC)*. IEEE, 2021, pp. 1811–1816.